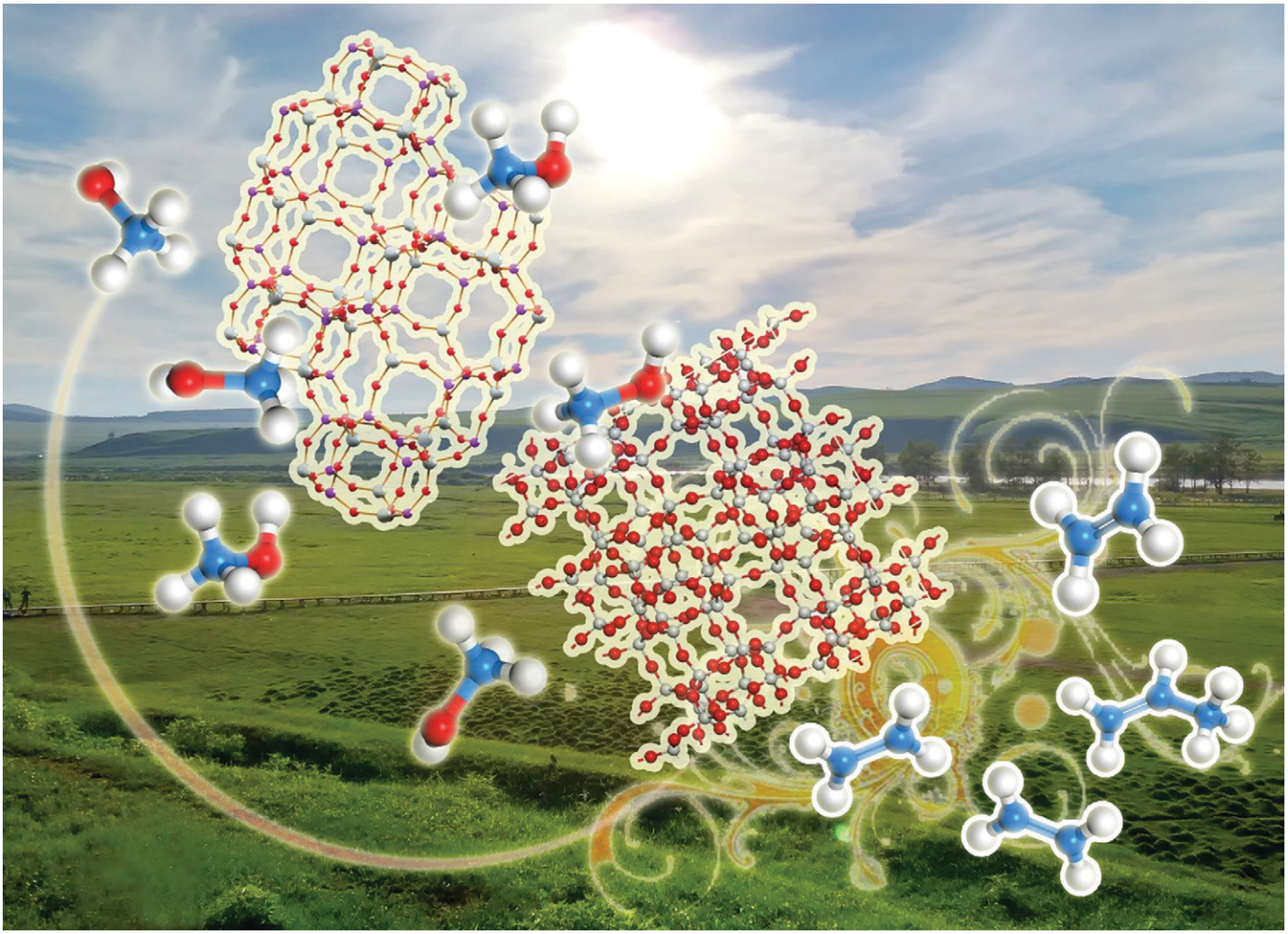

Showcasing research from Prof. Zhongmin Liu's team at Dalian Institute of Chemical Physics, Chinese Academy of Sciences, Dalian, China.

Comparative investigation of the deactivation behaviors over HZSM-5 and HSAPO-34 catalysts during low-temperature methanol conversion

At low reaction temperature, the deactivation of HZSM-5 originated from the "overloading effect" of methylbenzenes (smaller than pentamethylbenzene) which are intrinsically active during the autocatalysis reaction stage, while the deactivation of HSAPO-34 was caused by accumulation of the inactive methyladamantanes, which proceeded from "external to internal".

As featured in:

See Lei Xu, Zhongmin Liu *et al.*, *Catal. Sci. Technol.*, 2017, **7**, 2022.

ROYAL SOCIETY OF CHEMISTRY

rsc.li/catalysis

Registered charity number: 207890

Catalysis Science & Technology

PAPER

Cite this: *Catal. Sci. Technol.*, 2017, 7, 2022

Comparative investigation of the deactivation behaviors over HZSM-5 and HSAPO-34 catalysts during low-temperature methanol conversion†

Liang Qi,[ab] Jinzhe Li,[a] Linying Wang,[a] Chan Wang,[a] Lei Xu*[a] and Zhongmin Liu *[a]

Received 5th January 2017,
Accepted 31st March 2017

DOI: 10.1039/c7cy00024c

rsc.li/catalysis

The deactivation mechanism for the methanol conversion reaction at low temperature was comparatively investigated over HZSM-5 and HSAPO-34 catalysts. Two obviously different deactivation phenomena were directly observed: two-staged deactivation behavior over the HZSM-5 catalyst and exponential-type deactivation behavior over the HSAPO-34 catalyst. Since the start of the deactivation, the amount of the retained species over the HZSM-5 catalyst kept unchanged while the amount over the HSAPO-34 catalyst obviously increased. Both types of deactivation behavior presented an intimate relationship with the accumulation of retained species and their changing reactivity. After detailed characterization and analysis, it was interestingly found that the deactivation of the HZSM-5 catalyst originated from the "overloading effect" of methylbenzenes (smaller than pentamethylbenzene) which are intrinsically active during the autocatalysis reaction stage, while the deactivation of the HSAPO-34 catalyst was caused by accumulation of inactive methyladamantanes, and it was further deduced that the deactivation proceeded from "external to internal" for the HSAPO-34 catalyst. Enhancement of the catalyst diffusivity could effectively extend the catalyst lifetime for the HZSM-5 catalyst, but seemed less effective for the HSAPO-34 catalyst.

1. Introduction

Since the commercialization of the world's first MTO plant in Baotou, China, in 2010,[1,2] another 11 plants adopting the DMTO process developed by Dalian Institute of Chemical Physics have also been successfully put into stream up to 2016, providing China with a capability of 6460 kt y^{-1} of light olefins (ethene plus propene) in total. Currently, several other commercial methanol conversion processes such as methanol-to-gasoline (MTG), methanol-to-olefins (MTO), and methanol-to-propene (MTP) developed by different research organizations or companies have also achieved considerable progress.

There is no bound for the progress of science, and a better understanding of the reaction mechanism can help develop more efficient catalysts with higher target product selectivity and longer lifetimes in the future. The great success in commercialization has helped bring mechanistic studies to the core of MTH research, especially those that related to product formation and/or catalyst deactivation, which are still not well understood due to the complexity of the reaction system.[3,4] Nowadays, the "hydrocarbon pool" (HCP) mechanism is the most acceptable one for the methanol to hydrocarbon (MTH) reaction.[5–8] According to this mechanism, the organic compounds retained in the catalyst channels and/or intersections can act as reactive centers (namely HCP species), to which methanol are added and from which olefin products are eliminated.[5–10] Moreover, methylbenzenes and carbenium ions formed by the protonation of retained organics are generally regarded as the most important reaction intermediates.[4,11–22] Over catalysts like ZSM-5, ZSM-22 and ZSM-35, *etc.*, both polymethylbenzenes and olefins were proved to be active HCP species according to the "dual-cycle" mechanism, which was proposed as a modified version of the HCP mechanism.[7,8,23–25] In view of this acknowledgement, a lot of work has been carried out recently aiming at developing a catalyst with high target product selectivity by adjusting the contribution of alkene-based and aromatic-based reaction cycles.[23,26–28]

As a typical autocatalytic reaction, the MTH process is always accompanied by an obvious induction period which can be well interpreted through the HCP mechanism and it has been further proved that a certain amount of HCP species is needed to start apparent methanol conversion.[29] It is

[a] *National Engineering Laboratory for Methanol to Olefins, Dalian National Laboratory for Clean Energy, iChEM (Collaborative Innovation Center of Chemistry for Energy Materials), Dalian Institute of Chemical Physics, Chinese Academy of Sciences, Dalian 116023, People's Republic of China. E-mail: liuzm@dicp.ac.cn, leixu@dicp.ac.cn; Fax: +86 411 84379998; Tel: +86 411 84379998*

[b] *University of Chinese Academy of Sciences, Beijing 100049, People's Republic of China*

† Electronic supplementary information (ESI) available. See DOI: 10.1039/c7cy00024c

generally recognized that after the formation of the initial active species, more monocyclic and polycyclic compounds will subsequently be formed in an autocatalytic manner. During the autocatalysis or steady-state stage, besides the active retained species, some inactive and poorly mobile retained species and coke species will be unavoidably generated and strongly adsorb on Brønsted and Lewis acid sites and block pore entrances, leading to the final catalyst deactivation.[4,30,31] Moreover, it was recently found that the surface oxygen-containing cyclic species formed at the early stages of the MTH reaction also possessed an intimate relationship with the deactivating coke species.[32,33]

A lot of research has been done on the deactivation mechanism and it can be concluded that the deactivation behavior in various zeolite topologies is strongly influenced by the crystal size, acid site strength and acid concentration.[4,34–36] A nano-sized catalyst with lower acid site density and relatively weak acid strength usually possesses a longer life time.[4,34,36] The coking behavior and consequent deactivation are also obviously influenced by the zeolite pore structures.[32,37,38] HZSM-5 and HSAPO-34 are the best-known archetypal MTH catalysts which have already been successfully used for commercial methanol conversion. HZSM-5 is featured with the MFI topology, exhibiting a 3D network consisting of sinusoidal (5.1×5.5 Å^2) and straight (5.3×5.6 Å^2) 10-ring channels, resulting in medium-sized pores.[11] On the other hand, HSAPO-34 is a small-pore material, featuring the CHA topology, in which spacious cavities (10×6.7 Å^2) are connected by small (3.8×3.8 Å^2) 8-ring windows.[11] For the MTH reaction at high temperature, the coking behavior and the deactivation mechanism are different over the two porous structures: the presence of large cages in the CHA framework of HSAPO-34 could bring about much easier formation of bi- and polycyclic arenes in the cages and lead to fast deactivation, while in the MFI framework of HZSM-5 topologies, the channel intersections cannot accommodate polycyclic species that are too large and a longer catalyst lifetime could thereby be obtained.[4,37,39,40] Consequently, some researchers thought that the deactivation of HZSM-5 would be caused by the blocking of zeolite channels by the graphite-like coke formed on the external surface of the catalyst.[32]

Moreover, the deactivation mechanism is also strongly dependent on the reaction temperature,[2,8,41,42] we have found that over catalysts that have small cages like SAPO-35, SAPO-34 and SAPO-18, catalyst deactivation at low reaction temperatures was due to the formation of adamantane hydrocarbons, while the deactivation behavior at high temperature was caused by the accumulation of polycyclic aromatics.[2] Recently, it was found that over the HSSZ-13 zeolite, the main deactivating species were methylated naphthalene at low reaction temperatures (573–598 K) and heavier polycyclic species at high reaction temperatures (623–723 K).[43]

At low temperature, the coking behavior is relatively simple and identification of the active and deactivating species is easier.[20,44,45] For the HZSM-5 catalyst, it has been reported that the active species are tetramethylbenzenes (tetraMBs) and pentamethylbenzene (pentaMB) while the deactivating species are bulky and poorly mobile compounds like ethyltrimethylbenzenes and isopropyl-dimethylbenzenes at low temperature.[41,46,47] For the MTO reaction over the HSAPO-34 catalyst at low temperature, the deactivating species are methyladamantanes and the active species are methylbenzenes.[2] No matter what the deactivating species are and where they are located in the zeolite crystals, it has been conclusively recognized that the active HCP species could promote the catalyst activity while the inactive retained species or coke species would decrease the catalyst activity.[4,5]

However, we recently found that an "overloading effect" exists for lower-methylbenzenes (smaller than pentaMB) over HZSM-5 during the MTH reaction: too much accumulation of them in the catalyst channels will not greatly promote the methanol conversion, but will inversely lead to catalyst deactivation at low temperature due to the restricted catalyst diffusivity.[48] This finding made us reconsider the role of methylbenzenes and the MTH deactivation mechanism at low temperature. Moreover, for the MTH reaction at low temperature over HZSM-5 and HSAPO-34 catalysts, a quick deactivation phenomenon can always be observed immediately following the autocatalysis reaction,[2,3,29,35,45] indicating that the deactivation behavior under isothermal low temperature conditions should be also closely related to the active HCP species generated and accumulated in the autocatalysis reaction. Considering their different zeolite topology, reasons for the initiation of this deactivation behavior may not be the same over these two catalysts.

In the present work, the deactivation mechanism of the MTH reaction over HZSM-5 and HSAPO-34 catalysts at low reaction temperature was investigated. The role of the changing reactivity of the retained aromatics on the deactivation behavior was clearly revealed. After the autocatalysis stage, a two-staged deactivation behavior over HZSM-5 and an exponential-type deactivation behavior over HSAPO-34 were observed. With detailed characterization and analysis, these two deactivation phenomena were reasonably explained and it was found that, at low temperature, the deactivation of HZSM-5 originates from the overloaded HCP species while that of HSAPO-34 started from the blocking of the external surface by methyladamantanes.

2. Experimental section

2.1. Preparation of the catalysts

HZSM-5 samples (Si/Al = 19, 21) were obtained from the Catalyst Plant of Nankai University. The nano-crystalline ZSM-5 zeolite with a Si/Al ratio of 20 was synthesized according to a procedure in a previous report.[49] The three ZSM-5 samples were designated as MZ-19, MZ-21 and NZ-20 correspondingly.

Two SAPO-34 samples, one with an ordinary size and the other one nanosized (named as M-SAPO-34 and N-SAPO-34 correspondingly) were both supplied by Group DNL1202 of the Dalian Institute of Chemical Physics, Dalian, China. The

nano-crystalline SAPO-34 zeolite was synthesized according to a previous report.[50]

2.2. Characterization of the catalysts

The powder XRD pattern was recorded by a PANalytical X'Pert PRO X-ray diffractometer with Cu-Kα radiation (λ = 1.54059 Å), operating at 40 kV and 40 mA. The chemical composition of the samples was determined with a Philips Magix-601 X-ray fluorescence (XRF) spectrometer. The crystal morphology and structure was observed using a HITACHI SU8020 or S-3400 Scanning Electron Microscope.

N_2 adsorption–desorption isotherms were obtained on a Micrometrics ASAP 2020 system at 77 K.

The total amount of retained species in catalyst was determined using thermogravimetric analysis (TGA). Samples were firstly heated to 200 °C with a heating rate of 10 °C min^{-1}, and maintained for 10 min in an atmosphere of 20 mL min^{-1} N_2 to remove the physically adsorbed water. Then the atmosphere was changed to 10 mL min^{-1} O_2, combined with 10 mL min^{-1} N_2, and the sample was heated to 700 °C with a heating rate of 5 °C min^{-1}.

The nature of the organic compounds formed on the catalysts during the MTH reaction was monitored *in situ* by UV/vis spectroscopy which was carried out in the diffuse reflection mode in the range of 200–800 nm on a Varian Cary 5000 spectrophotometer. Prior to the studies, ~20 mg of the catalyst materials was finely ground and placed in the chamber. The samples were activated in flowing helium gas at 723 K for 1 h and cooled to the reaction temperature for taking a background spectrum. Then, methanol was fed by passing helium through a saturation evaporator and time-resolved spectra were recorded. The effluent product was analyzed with on-line mass spectra.

The change in the amount of retained species was also monitored *in situ* with an intelligent gravimetric analyzer (IGA) instrument, model IGA-003, Hiden Analytical Ltd., Warrington, UK. The sensitivity of the balance is 1 μg. Before the test, 100 mg of the catalyst materials (40–60 mesh) was placed in the chamber. The samples were pretreated in flowing helium gas until no decrease of the catalyst weight was observed, and adjusted to the reaction temperature. Then, methanol was fed by passing helium through a saturation evaporator and signals were recorded. The effluent product was analyzed with on-line mass spectra.

2.3. Catalytic studies

Methanol conversion was performed in a fixed-bed quartz tubular reactor at atmospheric pressure. A catalyst sample of 100 mg was loaded into the reactor and the catalyst was activated *in situ* with an air flow (20 mL min^{-1}) at 550 °C for 1 h before being adjusted to a predetermined reaction temperature and treated with flowing helium gas (20 mL min^{-1}) for 30 min. The methanol was fed by passing helium through a saturation evaporator with a WHSV of 2.0 h^{-1}. The reaction products were analyzed by on-line gas chromatography (Agilent GC 7890A) equipped with an HP-PLOT Q capillary column and a FID detector.

2.4. Extraction and GC-MS analysis of the confined organics

Organic compounds trapped in the catalyst were obtained by first dissolving the catalyst (50 mg) in 1.0 mL of 15% HF in a screw-cap Teflon vial. The organic phase was extracted by CH_2Cl_2 with 10 ppm C_2Cl_6 as internal standards, and then analyzed using an Agilent 7890A/5975C GC/MSD.

2.5. $^{12}C/^{13}C$-methanol switch experiments

In the $^{12}C/^{13}C$-methanol switch experiments, after ^{12}C-methanol was fed to the reactor by passing the carrier gas through a saturator for a predetermined time, the feeding of ^{12}C-methanol was stopped and the feeding line was switched to ^{13}C-methanol for a further 1.5 min. After that, the catalyst was cooled very quickly by putting it into a vessel containing liquid nitrogen. The isotopic distribution of the effluent products and the materials confined in the catalyst were determined by GC-MS (Agilent 7890/5975C).

3. Results and discussion

3.1. Characterization results of the HZSM-5 and HSAPO-34 catalysts.

Powder XRD confirmed that the three HZSM-5 samples consisted of a well crystalline MFI phase and the two HSAPO-34 catalysts consisted of a well crystalline CHA phase correspondingly (Fig. S1†). Fig. S2 and S3† show SEM photos of the HZSM-5 and HSAPO-34 catalysts. The MZ-19 sample possessed crystallite sizes of 1–2 μm, the MZ-21 sample possessed crystallite sizes of 2–3 μm while the NZ-20 sample was observed to have crystallite sizes of about 50 nm. For the M-SAPO-34 and N-SAPO-34 catalysts, the crystallite shapes were almost the same, but with obviously different crystallite sizes of about 10 μm and 200 nm correspondingly (Fig. S3†).

The BET results and chemical composition of the HZSM-5 and HSAPO-34 samples are given in Tables S1 and S2.† It can be seen that the external surface areas of the nano-sized HZSM-5 and HSAPO-34 samples were much higher than those of the micron-sized HZSM-5 and HSAPO-34 samples, demonstrating the enhanced diffusivity of the nano-sized catalysts.

The acidity of the HZSM-5 and HSAPO-34 samples measured by NH_3-TPD is presented in Fig. S4.† The TPD profiles for all the tested catalysts showed two desorption peaks at a low and a high temperature corresponding to weak and strong acid sites, respectively. For the MZ-19 sample, the desorption peak area below the TPD curve was a little higher than that of the MZ-21 and NZ-20 samples, implying the relatively higher acid site density, while the TPD curves for MZ-21 and NZ-20 were almost the same, indicating their similar acid character. The M-SAPO-34 and N-SAPO-34 catalysts also presented similar acid character.

3.2. The two-staged and the exponential-type deactivation behavior for HZSM-5 and HSAPO-34 catalysts

Methanol conversion reactions were performed over MZ-19 and M-SAPO-34 catalysts at low temperature (260–280 °C). The change of methanol conversion with time on stream (TOS) was carefully monitored during the whole reaction process for each reaction, and the results are shown in Fig. 1. An obvious induction period can be seen for both of the two catalysts at low temperature, which is consistent with previous work.[2,24,29] After that, for both samples, the methanol conversion increased rapidly during the subsequent autocatalysis stage but it suddenly dropped quickly once a maximum value was reached.

The product distribution from the autocatalysis stage to the deactivation stage was also continuously monitored and the results for both catalysts are shown in Fig. S5.† For MZ-19, the selectivity towards propene during the autocatalysis stage was much lower than that towards C_4, C_5 and C_{6+} products, but this increased rapidly immediately after the start of deactivation. Ethene and propene became the major products during the deactivation stage. For M-SAPO-34, the main products were always ethene and propene during the whole reaction progress, but the selectivity towards methane increased continuously in the final deactivation stage.

Moreover, it was clearly demonstrated that both the induction reaction and the deactivation reaction were obviously influenced by the reaction temperature for the two catalysts: a higher temperature could bring about not only a higher autocatalysis reaction rate but also a higher deactivation rate. This indicated that the formation of active and deactivating species and the relationships between them were very sensitive to the reaction temperature in the low temperature range. Moreover, although the deactivation behavior started soon after the autocatalysis stage, the observed deactivation phenomena were quite different for the two catalysts despite the similar reaction conditions. For the MZ-19 catalyst, the deactivation reaction can be divided into two stages: an initial quick deactivation stage and then a slow linear deactivation stage. In the latter stage, the deactivation rate is very slow and the HZSM-5 catalyst can sustain a low but relatively stable activity even after 10 hours of the MTH reaction (260 °C). For the M-SAPO-34 catalyst, the deactivation rate seems like an exponential function and the catalyst almost totally lost activity after 6 hours (260 °C).

Factors influencing the deactivation mechanism are very complex considering the HCP and "dual-cycle" mechanism and the changing diffusion properties of the catalyst channels and/or pores during the reaction process. Moreover, the accumulation of active and inactive species will not only influence the catalyst activity but also affect its diffusion characteristics which can further affect the product diffusion rate. In addition, the reactivity of the retained organic species may also change when the catalyst diffusivity became different. Further detailed characterization should be carried out to present a convincing reason for the different deactivation behavior of the two catalysts.

3.3. Change of catalyst physical properties and amount of retained species

After the MTH reaction proceeded to a predetermined time, the catalyst was cooled down rapidly with liquid nitrogen and the "coked" catalysts were characterized by BET and TG analysis. As is shown in Fig. 2, for MZ-19, the pore volume and the surface area decreased rapidly during the autocatalysis stage due to the quick accumulation of the retained species (Fig. 2(a)–(c)). According to general recognition, the amount of retained species may continuously increase from the

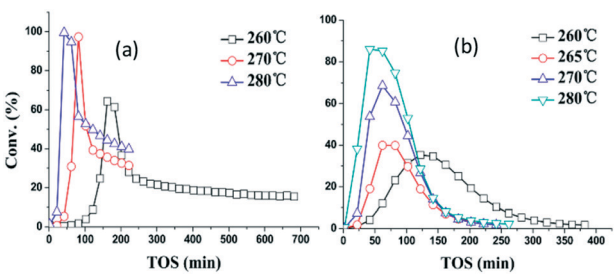

Fig. 1 Methanol conversion as a function of TOS at different temperature over MZ-19 (a) and M-SAPO-34 (b).

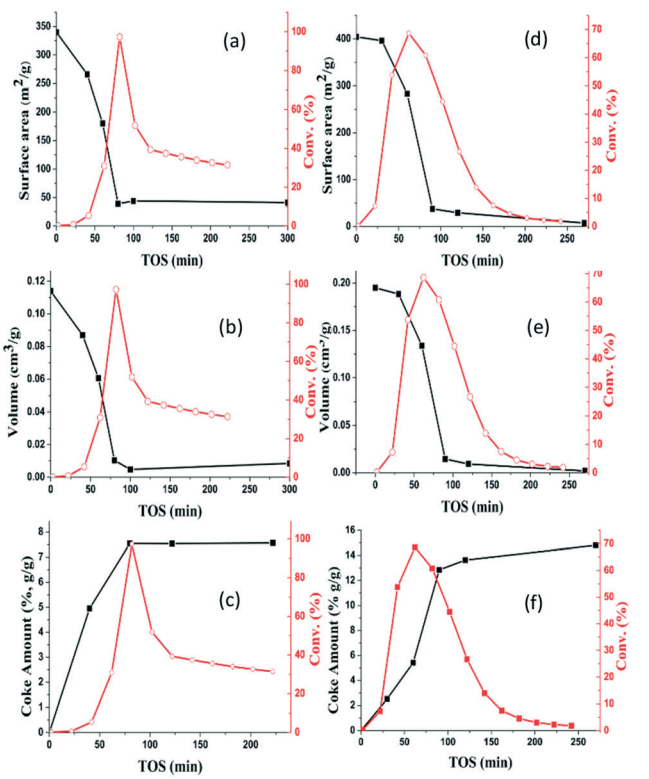

Fig. 2 Change of the catalyst surface area, volume and the amount of retained species with TOS at 270 °C for MZ-19 ((a)–(c)) and M-SAPO-34 ((d)–(f)).

autocatalysis to the deactivation stage whether they are active species or not. Moreover, the pore volume and the surface area may also keep decreasing. However, it is interesting to see that the pore volume, surface area and the amount of the retained species almost remained unchanged since the start of the deactivation stage. For the M-SAPO-34 catalyst, the changing trends of the pore volume and the surface area during the reaction process were obviously different. The pore volume and the surface area slightly decreased during the autocatalysis stage, while after that, the coke amount increased rapidly during the initial deactivation stage. During the whole deactivation stage, the rate of increase of the coke amount slowed down progressively but the amount of retained species increased continuously until the catalyst was completely deactivated. The pore volume and the surface area decreased to almost zero at the final deactivation stage for the M-SAPO-34 catalyst. As a result, it can be seen that for HZSM-5, almost all of the retained species were accumulated before deactivation, while for HSAPO-34, the major retained species were generated after the deactivation point. That is to say, although the deactivation started suddenly and rapidly at the end of the autocatalysis reaction for both catalysts, the coking behavior seemed to "accelerate" for HSAPO-34 but "stopped" for the HZSM-5 catalyst since the start of the deactivation.

3.4. GC-MS analysis of the retained species

GC-MS analysis was also carried out to investigate the changing composition of the retained organics during the whole reaction process. It can be seen from Fig. 3(a) that the major retained species were tetraMBs and pentaMB in very low concentrations at 40 min. The amount of tetraMBs and pentaMB increased greatly when the reaction proceeded to a time of 60 min and it later reached a maximum value at 80 min. It is worth noting that the dominant retained species was 1,2,3,5-tetraMB and the catalyst exhibited deactivation behavior at this point (Fig. 3(a)). Trimethylbenzenes (triMBs) and a small amount of methylnaphthalenes (MNs) can be detected after 80 min. During the deactivation stage, the concentration of MNs increased obviously as the reaction progressed.

The composition of the retained species over the HSAPO-34 catalyst at low reaction temperature was found to be quite different (Fig. 3(b)). The dominant retained species were methyladamantanes and the amount kept increasing after the start of the deactivation stage. pentaMB and hexamethylbenzene (hexaMB) have been proven to be the most important aromatic HCP species over SAPO-34 catalyst and only a small amount of them could be detected after 60 min which may be due to their high reactivity.[10,51] When the cages of the SAPO-34 catalyst were seriously blocked, a certain amount of triMBs and dimethylbenzenes (diMBs) were detected. The appearance of these lower methylbenzenes could be caused by the hindered methylation step during the deactivation stage.

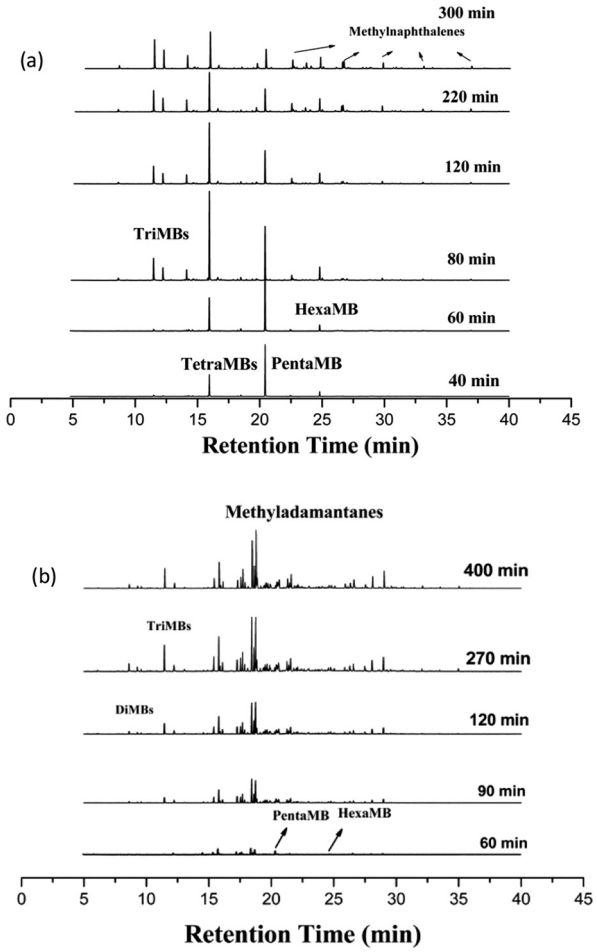

Fig. 3 GC-MS analysis of retained species after methanol conversion at 270 °C for MZ-19 (a) and M-SAPO-34 (b).

3.5. *In situ* UV/vis and IGA studies

UV/vis spectra were recorded over both samples during the MTH reaction (Fig. S6†). For both catalysts, all the UV/vis bands showed a rapid increase during the autocatalysis stage due to the quick accumulation of organic compounds. The obvious bands were at 260 and 280 nm for HZSM-5 and at 300 nm for the HSAPO-34 catalyst and these bands seem overlapped during the deactivation stage. On the basis of earlier UV/vis studies of organic compounds on acidic zeolite catalysts,[22,52–56] the bands at 260 and 280 nm were assigned to UV/vis-sensitive dienes and polyalkylaromatics,[56] respectively. According to the earlier recognition of the retained species in HSAPO-34 after a low temperature MTH reaction (Fig. 3(b)),[2] the bands at 300 nm may be due to the accumulation of methyladamantanes. To clearly observe the change of the UV/vis bands, the signals of these bands were extracted and plotted against time on steam together with the change of ethene mass spectrometry signal (Fig. 4). It can be seen clearly that for the HZSM-5 catalyst, the intensity of the two bands firstly increased rapidly and then kept constant from the beginning of the deactivation stage (Fig. 4(a)). For the

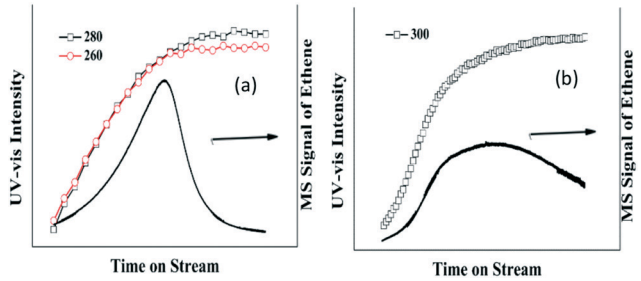

Fig. 4 Signal recorded during the *in situ* UV/vis analysis in the MTH reaction at 270 °C over MZ-19 (a) and M-SAPO-34 (b).

HSAPO-34 catalyst, the intensity of the chosen bands continuously increased from the autocatalysis to the deactivation stage (Fig. 4(b)). The UV-vis results corresponded with the characterization results in Fig. 2 very well and could be correlated with the evolution of methanol conversion with temperature.

The change of the amount of the retained species was further monitored with the IGA analysis for both catalysts (Fig. 5). Similarly to the *in situ* UV-vis result, it was again found that the amount of the retained species kept constant from the beginning of the deactivation stage for the HZSM-5 catalyst, and for the HSAPO-34 catalyst, the amount of the retained species continued to increase from the beginning of the deactivation stage.

3.6. Low-temperature deactivation mechanism for HZSM-5 and HSAPO-34.

3.6.1 Deactivation mechanism for HZSM-5. It is generally recognized that the deactivation behavior is caused by the accumulation of too many inactive retained species, the amount of which may continue to increase during the deactivation stage. However, according to the above characterization results, the major retained species after the beginning of the deactivation stage was methylbenzenes, which have been proved to be the active HCP species during the MTH reaction over HZSM-5.[46,47] GC-MS analysis of the retained species was also performed for the MTH reaction at 280 °C to further consolidate this finding and the evolution of the retained species seemed the same as that observed at 270 °C (Fig. S7†). This is different to former reports of the deactivation of HZSM-5 at low reaction temperatures which ascribed the deactivation behaviour to the accumulation of bulky and poorly mobile compounds like ethyl-trimethylbenzenes and isopropyl-dimethylbenzenes.[30,41] As a result, the low-temperature deactivation behavior over HZSM-5 seemed confusing at first sight. Moreover, it should be noted that the total amount of the retained species kept constant during the deactivation stage. So, it can be deduced that the deactivation may be induced by the decreasing reactivity of the retained methylbenzenes.

$^{12}C/^{13}C$-methanol switch experiments were carried out as the reaction progressed at 280 °C to monitor the changing reactivity of the retained species. The total ^{13}C content of the retained organic materials and effluent alkenes after the switch experiments are shown in Fig. 6. At TOS = 30 min, tetraMBs and pentaMB exhibited a higher ^{13}C content than the other organic materials retained in HZSM-5, implying their high reactivity as important intermediates during the autocatalysis stage.[46,47] However, it can be seen clearly that the reactivity of the retained aromatics started to decrease before the deactivation stage. After the start of the deactivation, the reactivity of triMBs and tetraMBs continued decreasing rapidly while pentaMB and hexaMB started to recover their reactivity. The reactivity of all the retained species almost kept unchanged during the slowly linear deactivation stage. As for the effluent alkenes (Fig. 6(b)), the ^{13}C content was lower than that of the retained aromatics when TOS = 30 min and it continued to decrease at the deactivating point. After that, the ^{13}C content of the alkene products increased rapidly during the initial rapid deactivation stage and then all of them almost kept constant during the slow linear deactivation stage. Considering the results of the isotopic switch experiment, it can be deduced that the MTH reaction mainly follows the aromatic-based cycle and then switches to the olefin-based cycle during the deactivation stage.

In the later autocatalysis reaction stage (before the maximum methanol conversion), the reactivity of the aromatics has already started to decrease due to the shrinking internal space caused by the continuously increasing amount of retained species. At the same time, the amount of retained

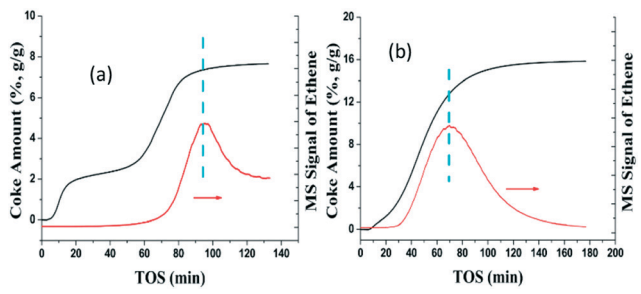

Fig. 5 IGA studies in the MTH reaction at 275 °C over MZ-19 (a) and M-SAPO-34 (b).

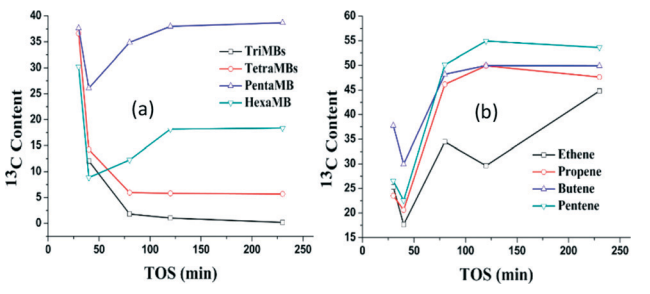

Fig. 6 The total ^{13}C content of the retained organic materials (a) and the effluent products (b) after the $^{12}C/^{13}C$ switch experiment over MZ-19 during the MTH reaction at 280 °C. The switch experiments were performed with ^{12}C-methanol feeding for 30, 40, 80, 120 and 240 min respectively, followed by 1.5 min of ^{13}C-methanol feeding.

methylbenzenes also increased greatly in this stage. For the total reactivity, the increasing rate was higher than the decreasing rate, so the total apparent reactivity of all the retained species continued to increase. Thereafter, the amount of the total retained species kept constant from the beginning of the deactivation stage, the reactivity of tetraMBs and triMBs continued decreasing and pentaMB and hexaMB gradually recovered their reactivity. At the same time, the inactive methylbenzenes smaller than tetraMBs became the dominant retained species during the deactivation stage and consequently, the catalyst activity decreased rapidly.

The reactivity of pentaMB and hexaMB seemed almost unchanged during the deactivation stage, and considering the molecular size of pentaMB and hexaMB, most of them possibly existed near the external surface of HZSM-5 crystals. The decreasing reactivity at 40 min may be caused by those that exist in the zeolite channels, which were then cracked to inactive smaller methylbenzenes.

According to the isotopic switching experiment, it can be seen clearly that it was the sudden loss of the reactivity of the retained aromatics that led to the initial rapid deactivation; namely, the initial deactivation stage was caused by the "overloading effect" of HCP compounds (Scheme 1). During the second deactivation stage, pentaMB and hexaMB were still active and can be further transformed into lower active methylnaphthalenes. But this step is very slow and is difficult to proceed at low temperature, so the corresponding deactivating rate is rather slow and the MTH reaction switched to the olefin-based cycle.

3.6.2 Deactivation mechanism for HSAPO-34. It has been reported that at low temperature, the accumulation of diamondoid hydrocarbons, which are inactive species, could lead to pore blockage and finally result in the deactivation of HSAPO-34,[2] and this corresponds with the current analysis very well. However, it should be noted that, the rapid increase of the amount of methyladamantanes and the quick decrease of the catalyst pore volume and surface area occurred right after the start of the deactivation behavior, which is obviously different from the coking behavior observed over the HZSM-5 catalyst.

From the $^{12}C/^{13}C$ switch experiment result (Fig. 7) it can be seen that the higher methylbenzenes were still very active at the beginning of the deactivation stage but the reactivity decreased quickly as the reaction progressed on. As for the alkene products, the ^{13}C content first increased which may be due to the enhancement of the olefin-based cycle during the deactivation process, and then it decreased again because of the seriously blocked catalyst channels and cages.

It has been reported that the distribution of Si atoms in the crystals was non-uniform, and there exists a gradual increase from the core to the surface.[1] Moreover, it is reasonable to speculate that the stronger acidic sites on the external surface would have high priority for the formation of retained species. Considering the non-uniformly distributed acidic sites along the crystals and the characterization results of the deactivated SAPO-34, the deactivation behavior over SAPO-34 can be understood as "proceeding from external to internal" (Scheme 2). A certain amount of methyladamantanes, firstly formed in the cages at the surface of the crystals, may cause diffusion limitation and inhibit the release of product generated inside. At the same time, the retained higher methylbenzenes are still very active and continue working to generate olefin products inside the surface-blocked SAPO-34 crystals. However, it is difficult for the olefin products to diffuse out due to the reduced catalyst diffusion properties. Consequently, the generation and accumulation of methyladamantanes would be accelerated in the initial deactivation stage. As the reaction proceeds on, both the internal space and the reactivity of the methylbenzenes continuously decrease. As a result, the formation rate of methyladamantanes decreases and the deactivation rate slows down.

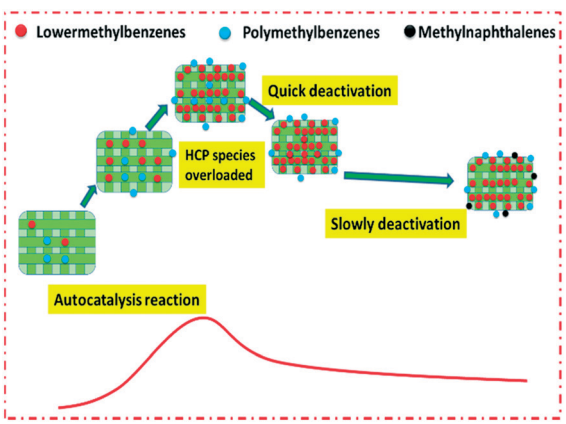

Scheme 1 Explanation of the low-temperature MTH deactivation mechanism over HZSM-5.

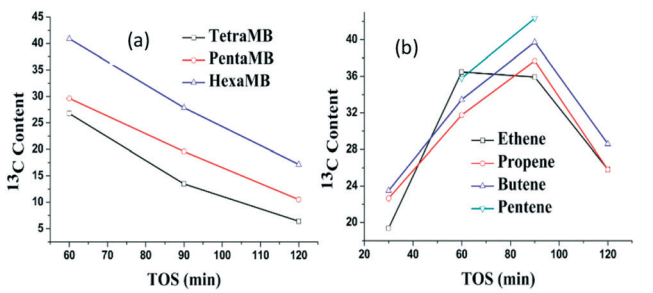

Fig. 7 The total ^{13}C content of the retained organic materials (a) and the effluent products (b) after the $^{12}C/^{13}C$ switch experiment over M-SAPO-34 during the MTH reaction at 280 °C. The switch experiments were performed with ^{12}C-methanol feeding for 60, 90 and 120 min respectively for (a), followed by 1.5 min of ^{13}C-methanol feeding. The switch experiments were performed with ^{12}C-methanol feeding for 30, 60, 90 and 120 min respectively for (b), followed by 1.5 min of ^{13}C-methanol feeding.

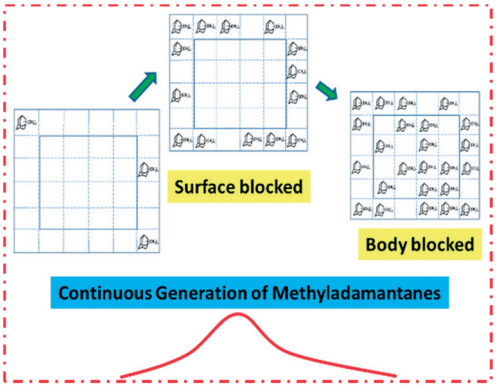

Scheme 2 Illustration of the formation of methyladamantanes under low-temperature MTH reaction over HSAPO-34.

3.7. Deactivation behavior over catalysts with enhanced diffusivity

With clear recognition of the deactivation mechanism, we proposed that the deactivation behavior may be influenced by the catalyst diffusivity which is closely related to the external surface area. As a result, nano-range crystal size ZSM-5 (NZ-20) and SAPO-34 (N-SAPO-34) samples were synthesized. According to the NH_3-TPD result in Fig. S4† (a), the acid site density of MZ-19 catalyst was relatively higher than that of the NZ-20 catalyst. For a better comparison, an MZ-21 catalyst with similar acid character but a different crystal size to NZ-20 was also selected. The external surface areas of the nano-sized samples were much higher than the conventional ones, indicating their better diffusion characteristics (Tables S1 and S2†).

The methanol conversion reactions were performed over the MZ-21, NZ-20 and N-SAPO-34 catalysts. The MTH reaction behavior over MZ-21 was similar to that over the MZ-19 catalyst (Fig. S8†), and quick deactivation behavior was observed right after the autocatalysis stage. For the NZ-20 catalyst, the induction period can be observed at 260 and 270 °C followed by an obvious autocatalysis reaction and this phenomenon was almost the same as that over the MZ-19 catalyst. However, it can be seen clearly that no obvious deactivation behavior was presented after the autocatalysis reaction and only a very slight decrease of methanol conversion can be observed (Fig. 8(a)). The amount of the retained species was much lower than that observed over the MZ-19 catalyst (only 3.4 wt%) (Fig. 8(c)). Combined with the $^{12}C/^{13}C$ switch experiment and the GC-MS analysis, it can be seen that the major retained species were pentaMB and tetraMBs, and both of them were very active even after 240 min of MTH reaction at 270 °C. The shorter diffusion path length promoted the diffusion of the effluent products and further prevented the aggregation of too many retained species and helped diminish the "overloading effect". Consequently, the lifetime of the catalyst at low temperature could be largely extended. However, the enhanced catalyst diffusivity and the large external surface area seemed less effective at extending the lifetime of the SAPO-34 catalyst (Fig. 9), and obvious deactivation behavior was observed over the N-SAPO-34 catalyst. This indicated that the generation of methyladamantanes was very easy in the SAPO-34 cages, even over catalysts with enhanced diffusivity.

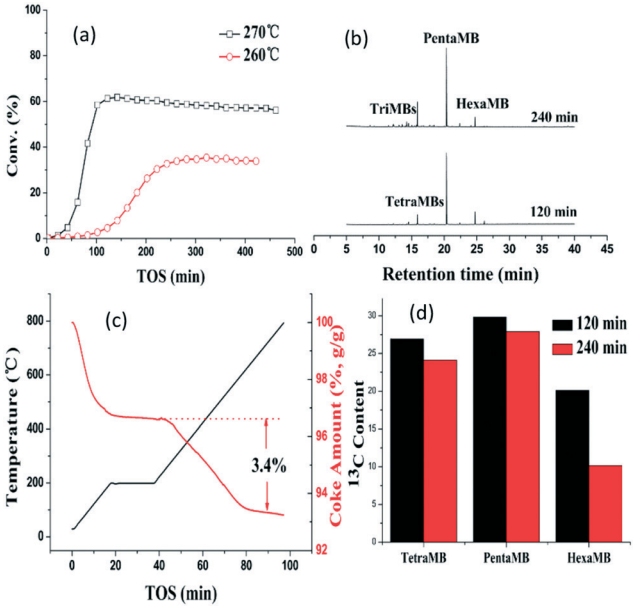

Fig. 8 Methanol conversion as a function of TOS at different temperature over NZ-20 catalyst (a), GC-MS analysis of retained species after methanol conversion at 270 °C for 120 and 240 min over NZ-20 catalyst (b), TG analysis of the catalyst after 240 min methanol conversion at 270 °C over NZ-20 catalyst (c), the total ^{13}C content of the retained organic materials after the $^{12}C/^{13}C$ switch experiment over NZ-20 catalyst at 270 °C, with ^{12}C-methanol feeding during the MTH reaction for 120 and 240 min, followed by 1.5 min of ^{13}C-methanol feeding (d).

3.8. Discussion of the different deactivation behavior over HZSM-5 and HSAPO-34

Based on the above investigations, it may be recognized that the low temperature deactivation behavior over HZSM-5 and

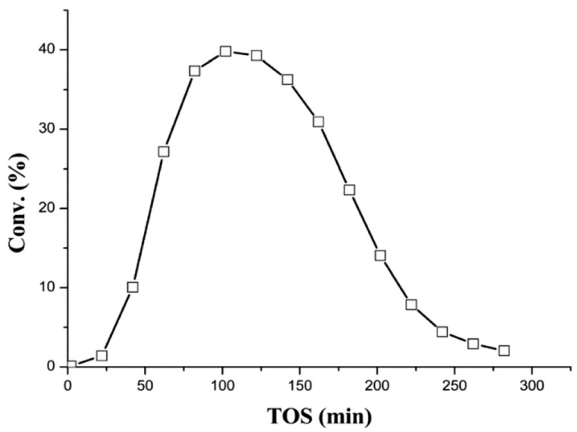

Fig. 9 Methanol conversion as a function of TOS at 270 °C over N-SAPO-34 catalyst.

HSAPO-34 was both due to the high occupation of the internal space of the catalyst, despite the different composition of the retained species. As a result, not enough space was left for the proceeding of HCP cycles and it also became difficult for the HCP species and methanol molecules to get access to the internal acid sites.

It is clearly seen that, in the deactivation stage, the major retained species for the HZSM-5 and HSAPO-34 catalysts were methylbenzenes and methyladamantanes respectively. One of these is the intrinsically active HCP species, and the other one is an inactive species. The formation of different retained species was due to the different catalyst topologies and it seems that, at low temperature, catalysts with 10-ring channels or channel intersections are more likely to form methylbenzenes,[24,25,57,58] while catalysts with a cage-type topology are more apt at generating methyladamantanes.[2,35,59] The process of occupation of the catalyst internal space is quite different for the two catalysts. For HZSM-5, the overloaded methylbenzenes accumulated due to their autocatalytic generation in the autocatalysis stage and almost all of the retained species were formed before the deactivation point. For HSAPO-34, a relatively small amount of methylbenzenes could be retained in the autocatalysis stage which may be caused by their higher activity. Alternatively, a certain amount of inactive methyladamantanes was preferentially generated and was retained in the cages near the external surface.

In the latter deactivation stage, the total amount of the retained species in HZSM-5 almost kept unchanged but the retained methylbenzenes were slowly transformed into the less active methylnaphthalenes.[58] However, this step proceeded very slowly and is difficult at low temperature, so the corresponding deactivation rate is rather slow and the MTH reaction mainly switches to the olefin-based cycle. For the HSAPO-34 catalyst, after the blocking of the external channels and cages, much more inactive species would be generated in an accelerating rate. Consequently, the amount of the methyladamantanes increased continuously in the deactivation stage over the HSAPO-34 catalyst.

With the synthesized HZSM-5 catalyst with enhanced diffusion properties, the "overloading effect" of methylbenzene could be alleviated and the lifetime of the catalyst can be effectively extended at low temperature. However, the same method seemed less effective for the HSAPO-34 catalyst. That is because the main reason for the deactivation over HSAPO-34 is the formation of methyadamantanes, and the enhancement of the catalyst diffusivity can not prevent its generation. It may be proposed that, if we can think of a method that can prevent the formation of methyladamantanes, the lifetime of the HSAPO-34 catalyst could be greatly extended at low temperature.

4. Conclusions

The deactivation mechanism for the MTH reaction at low temperature over HZSM-5 and HSAPO-34 catalysts was comparatively investigated. Over these two catalysts, the deactivation behavior was quite different: two-staged deactivation behavior over HZSM-5 and exponential-type deactivation behavior over HSAPO-34 was clearly observed. It was further found that the amount of the retained species kept unchanged over the HZSM-5 catalyst but kept increasing over HSAPO-34 catalyst from the beginning of the deactivation. The role of the changing reactivity of the retained aromatics in the deactivation was revealed. With detailed characterization and analysis, it was concluded that the deactivation of the HZSM-5 catalyst originated from the "overloading effect" of methylbenzenes while the deactivation of HSAPO-34 was caused by accumulation of the inactive methyladamantanes. In the deactivation stage, the retained species in HZSM-5 were slowly transformed into the less active methylnaphthalenes and the MTH reaction mainly switched to the olefin-based cycle. For the HSAPO-34 catalyst, after the blocking of the external channels and cages, much more methyladamantanes would be generated in an accelerating rate in the initial deactivation stage and the total coke amount increased continuously over HSAPO-34. Furthermore, with the nano-sized ZSM-5 catalyst, on which the "overloading effect" of methylbenzenes can be avoided, the deactivation behavior was eliminated. However, the formation of the methyladamantanes cannot be avoided even over nano-sized HSAPO-34 with enhanced diffusivity, and deactivation behavior was still obvious over the synthesized nano-sized HSAPO-34 catalyst.

Acknowledgements

The authors thank financial support from the National Natural Science Foundation of China (No. 21576256 and No. 21273005), and Dr Miao Yang for sample characterization and beneficial discussion.

Notes and references

1 P. Tian, Y. X. Wei, M. Ye and Z. M. Liu, *ACS Catal.*, 2015, **5**, 1922–1938.
2 Y. X. Wei, J. Z. Li, C. Y. Yuan, S. T. Xu, Y. Zhou, J. R. Chen, Q. Y. Wang, Q. Zhang and Z. M. Liu, *Chem. Commun.*, 2012, **48**, 3082–3084.
3 M. Stocker, *Microporous Mesoporous Mater.*, 1999, **29**, 3–48.
4 U. Olsbye, S. Svelle, M. Bjorgen, P. Beato, T. V. W. Janssens, F. Joensen, S. Bordiga and K. P. Lillerud, *Angew. Chem., Int. Ed.*, 2012, **51**, 5810–5831.
5 J. F. Haw, W. G. Song, D. M. Marcus and J. B. Nicholas, *Acc. Chem. Res.*, 2003, **36**, 317–326.
6 I. M. Dahl and S. Kolboe, *J. Catal.*, 1994, **149**, 458–464.
7 S. Svelle, F. Joensen, J. Nerlov, U. Olsbye, K. P. Lillerud, S. Kolboe and M. Bjorgen, *J. Am. Chem. Soc.*, 2006, **128**, 14770–14771.
8 M. Bjorgen, S. Svelle, F. Joensen, J. Nerlov, S. Kolboe, F. Bonino, L. Palumbo, S. Bordiga and U. Olsbye, *J. Catal.*, 2007, **249**, 195–207.
9 I. M. Dahl and S. Kolboe, *Catal. Lett.*, 1993, **20**, 329–336.

10 W. G. Song, J. F. Haw, J. B. Nicholas and C. S. Heneghan, *J. Am. Chem. Soc.*, 2000, **122**, 10726–10727.
11 K. Hemelsoet, J. Van der Mynsbrugge, K. De Wispelaere, M. Waroquier and V. Van Speybroeck, *ChemPhysChem*, 2013, **14**, 1526–1545.
12 S. Ilias and A. Bhan, *J. Catal.*, 2012, **290**, 186–192.
13 K. De Wispelaere, K. Hemelsoet, M. Waroquier and V. Van Speybroeck, *J. Catal.*, 2013, **305**, 76–80.
14 M. Westgard Erichsen, S. Svelle and U. Olsbye, *J. Catal.*, 2013, **298**, 94–101.
15 S. Ilias and A. Bhan, *J. Catal.*, 2014, **311**, 6–16.
16 T. Xu and J. F. Haw, *J. Am. Chem. Soc.*, 1994, **116**, 7753–7759.
17 T. Xu, D. H. Barich, P. W. Goguen, W. G. Song, Z. K. Wang, J. B. Nicholas and J. F. Haw, *J. Am. Chem. Soc.*, 1998, **120**, 4025–4026.
18 W. G. Song, H. Fu and J. F. Haw, *J. Phys. Chem. B*, 2001, **105**, 12839–12843.
19 W. G. Song, J. B. Nicholas and J. F. Haw, *J. Phys. Chem. B*, 2001, **105**, 4317–4323.
20 S. T. Xu, A. M. Zheng, Y. X. Wei, J. R. Chen, J. Z. Li, Y. Y. Chu, M. Z. Zhang, Q. Y. Wang, Y. Zhou, J. B. Wang, F. Deng and Z. M. Liu, *Angew. Chem., Int. Ed.*, 2013, **52**, 11564–11568.
21 W. O. Haag, R. M. Lago and P. G. Rodewald, *J. Mol. Catal.*, 1982, **17**, 161–169.
22 W. L. Dai, M. Scheibe, L. D. Li, N. J. Guan and M. Hunger, *J. Phys. Chem. C*, 2012, **116**, 2469–2476.
23 X. Y. Sun, S. Mueller, H. Shi, G. L. Haller, M. Sanchez-Sanchez, A. C. van Veen and J. A. Lercher, *J. Catal.*, 2014, **314**, 21–31.
24 L. Qi, J. Z. Li, L. Xu and Z. M. Liu, *RSC Adv.*, 2016, **6**, 56698–56704.
25 J. B. Wang, Y. X. Wei, J. Z. Li, S. T. Xu, W. N. Zhang, Y. L. He, J. R. Chen, M. Z. Zhang, A. M. Zheng, F. Deng, X. W. Guo and Z. M. Liu, *Catal. Sci. Technol.*, 2016, **6**, 89–97.
26 S. Ilias and A. Bhan, *ACS Catal.*, 2013, **3**, 18–31.
27 P. Kumar, J. W. Thybaut, S. Svelle, U. Olsbye and G. B. Marin, *Ind. Eng. Chem. Res.*, 2013, **52**, 1491–1507.
28 X. Y. Sun, S. Mueller, Y. Liu, H. Shi, G. L. Haller, M. Sanchez-Sanchez, A. C. van Veen and J. A. Lercher, *J. Catal.*, 2014, **317**, 185–197.
29 L. Qi, Y. X. Wei, L. Xu and Z. M. Liu, *ACS Catal.*, 2015, **5**, 3973–3982.
30 H. Schulz, *Catal. Today*, 2010, **154**, 183–194.
31 D. Mores, E. Stavitski, M. H. F. Kox, J. Kornatowski, U. Olsbye and B. M. Weckhuysen, *Chem. – Eur. J.*, 2008, **14**, 11320–11327.
32 S. Muller, Y. Liu, M. Vishnuvarthan, X. Y. Sun, A. C. van Veen, G. L. Haller, M. Sanchez-Sanchez and J. A. Lercher, *J. Catal.*, 2015, **325**, 48–59.
33 Y. Liu, S. Muller, D. Berger, J. Jelic, K. Reuter, M. Tonigold, M. Sanchez-Sanchez and J. A. Lercher, *Angew. Chem., Int. Ed.*, 2016, **55**, 5723–5726.
34 W. L. Dai, G. J. Wu, L. D. Li, N. J. Guan and M. Hunger, *ACS Catal.*, 2013, **3**, 588–596.
35 J. R. Chen, J. Z. Li, C. Y. Yuan, S. T. Xu, Y. X. Wei, Q. Y. Wang, Y. Zhou, J. B. Wang, M. Z. Zhang, Y. L. He, S. L. Xu and Z. M. Liu, *Catal. Sci. Technol.*, 2014, **4**, 3268–3277.
36 G. J. Yang, Y. X. Wei, S. T. Xu, J. R. Chen, J. Z. Li, Z. M. Li, J. H. Yu and R. R. Xu, *J. Phys. Chem. C*, 2013, **117**, 8214–8222.
37 M. Guisnet and P. Magnoux, *Appl. Catal.*, 1989, **54**, 1–27.
38 M. Guisnet and P. Magnoux, *Appl. Catal., A*, 2001, **212**, 83–96.
39 S. Bhatia, J. Beltramini and D. D. Do, *Catal. Rev.: Sci. Eng.*, 1989, **31**, 431–480.
40 R. Y. Brogaard, B. M. Weckhuysen and J. K. Norskov, *J. Catal.*, 2013, **300**, 235–241.
41 H. Schulz and M. Wei, *Microporous Mesoporous Mater.*, 1999, **29**, 205–218.
42 T. Behrsing, H. Jaeger and J. V. Sanders, *Appl. Catal.*, 1989, **54**, 289–302.
43 E. Borodina, F. Meirer, I. Lezcano-Gonzalez, M. Mokhtar, A. M. Asiri, S. A. Al-Thabaiti, S. N. Basahel, J. Ruiz-Martinez and B. M. Weckhuysen, *ACS Catal.*, 2015, **5**, 992–1003.
44 J. Z. Li, Y. X. Wei, J. R. Chen, P. Tian, X. Su, S. T. Xu, Y. Qi, Q. Y. Wang, Y. Zhou, Y. L. He and Z. M. Liu, *J. Am. Chem. Soc.*, 2012, **134**, 836–839.
45 J. Z. Li, Y. X. Wei, J. R. Chen, S. T. Xu, P. Tian, X. F. Yang, B. Li, J. B. Wang and Z. M. Liu, *ACS Catal.*, 2015, **5**, 661–665.
46 C. Wang, Y. Y. Chu, A. M. Zheng, J. Xu, Q. Wang, P. Gao, G. D. Qi, Y. J. Gong and F. Deng, *Chem. – Eur. J.*, 2014, **20**, 12432–12443.
47 C. Wang, J. Xu, G. D. Qi, Y. J. Gong, W. Y. Wang, P. Gao, Q. Wang, N. D. Feng, X. L. Liu and F. Deng, *J. Catal.*, 2015, **332**, 127–137.
48 L. Qi, J. Z. Li, L. Y. Wang, L. Xu and Z. M. Liu, *Catal. Sci. Technol.*, 2017, **7**, 894–901.
49 M. Abrishamkar and A. Izadi, *Microporous Mesoporous Mater.*, 2013, **180**, 56–60.
50 M. Yang, P. Tian, C. Wang, Y. Y. Yuan, Y. Yang, S. T. Xu, Y. L. He and Z. M. Liu, *Chem. Commun.*, 2014, **50**, 1845–1847.
51 B. Arstad and S. Kolboe, *J. Am. Chem. Soc.*, 2001, **123**, 8137–8138.
52 J. Huang, Y. Jiang, V. R. Marthala, Y. S. Ooi, J. Weitkarnp and M. Hunger, *Microporous Mesoporous Mater.*, 2007, **104**, 129–136.
53 Y. J. Jiang, J. Huang, V. R. R. Marthala, Y. S. Ooi, J. Weitkamp and M. Hunger, *Microporous Mesoporous Mater.*, 2007, **105**, 132–139.
54 W. L. Dai, M. Scheibe, N. J. Guan, L. D. Li and M. Hunger, *ChemCatChem*, 2011, **3**, 1130–1133.
55 W. L. Dai, X. Wang, G. J. Wu, N. J. Guan, M. Hunger and L. D. Li, *ACS Catal.*, 2011, **1**, 292–299.
56 M. Bjorgen, F. Bonino, S. Kolboe, K. P. Lillerud, A. Zecchina and S. Bordiga, *J. Am. Chem. Soc.*, 2003, **125**, 15863–15868.
57 L. Qi, J. Z. Li, Y. X. Wei, Y. L. He, L. Xu and Z. Liu, *RSC Adv.*, 2016, **6**, 52284–52291.
58 L. Qi, J. Z. Li, Y. X. Wei, L. Xu and Z. M. Liu, *Catal. Sci. Technol.*, 2016, **6**, 3737–3744.
59 J. R. Chen, J. Z. Li, Y. X. Wei, C. Y. Yuan, B. Li, S. T. Xu, Y. Zhou, J. B. Wang, M. Z. Zhang and Z. M. Liu, *Catal. Commun.*, 2014, **46**, 36–40.